Modeling and Simulation of Bio-Inspired Nanoarmors

Stefano Signetti and Nicola M. Pugno

Contents

S. Signetti (✉)
Laboratory of Bio-Inspired and Graphene Nanomechanics, Department of Civil, Environmental and Mechanical Engineering, University of Trento, Trento, Italy

Currently at: Department of Mechanical Engineering, Korea Advanced Institute of Science and Technology (KAIST), Daejeon, Republic of Korea
e-mail: ssignetti@kaist.ac.kr

N. M. Pugno (✉)
Department of Mechanical Engineering, Korea Advanced Institute of Science and Technology (KAIST), Daejeon, Republic of Korea

School of Engineering and Materials Sciences, Queen Mary University of London, London, UK

Ket-Lab, Edoardo Amaldi Foundation, Italian Space Agency, Rome, Italy
e-mail: nicola.pugno@unitn.it

C.-H. Hsueh et al. (eds.), *Handbook of Mechanics of Materials*,
https://doi.org/10.1007/978-981-10-6855-3_15-1

Abstract

The exploitation of bio-inspired solutions and of novel nanomaterials is gaining increasing attention in the field of impact protection. Indeed, especially for advanced applications, there is a growing pressure towards the reduction of the weight of protective structures without compromising their energy absorption capability. The complexity of the phenomena induced by high-energy contacts requires advanced and efficient computational models, which are also fundamental for achieving the optimum, overcoming the limits of experimental tests and physical prototyping in exploring the whole design space. At the same time, the modeling of bio-inspired toughening mechanisms requires additional capability of these methods to efficiently cover and merge different -and even disparate- size and time scales. In this chapter, we review computational methods for modeling the mechanical behavior of materials and structures under high-velocity (e.g., ballistic) impacts and crushing, with a particular focus on the nonlinear finite element method. Some recent developments in numerical simulation of impact are presented underlining merits, limits, and open problems in the modeling of bio-inspired and nanomaterial-based armors. In the end, two modeling examples, a bio-inspired ceramic-composite armor with ballistic protection capabilities and a modified honeycomb structure for energy absorption, are proposed.

1 Introduction

The understanding of impact behavior of materials and structures is of extreme importance in a wide range of engineering and technological applications. Among all, the protection of space vehicles from the impact of micrometeoroids or orbital space debris [1] represents one of the most challenging applications due to the high impact velocities of the smallest micrometric debris (the velocity of low Earth orbiting satellites is about 7–8 km/s, but the relative impact speed may be higher) and to their consequent high penetration capability. Other important requirements in space structures are an extreme resilience of vital systems, since multiple faults are not allowed in space missions (Fig. 1), and the limit of the overall mass due to related rocket transportation capabilities and costs. These engineering goals are always in competition, with the result that a compromise with the acceptable level of risk of failure must be reached. Thus, the design does not limit to the mere maximization of protection, which would be straightforwardly achievable with a massive armor.

For some decades, the answer to these tasks has been – and still largely is – the adoption of composite materials [2, 3] based on the combination of synthetic fibers (e.g., Kevlar®, Dyneema®) and thermoset resin that has allowed to effectively reach protection levels and low weights previously unimaginable with metallic targets. However, the aging and degradation of these materials, especially in extreme environments, must be properly assessed [4, 5]. When dealing with high penetrating projectiles, a hard ceramics front layer may also be employed: impactors are first blunted and worn down by the ceramic which also spreads the load over a larger area; then, the composite

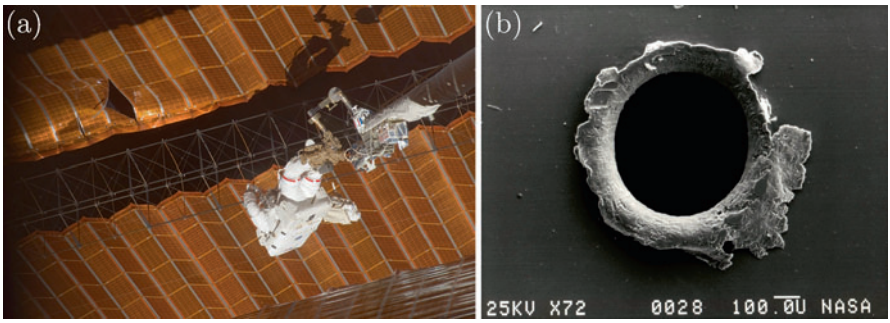

Fig. 1 Damage on the International Space Station by micrometeoroid impact. (**a**) Astronaut Scott Parazynski during extravehicular activity (EVA) on 3rd November 2007 to make a critical repair on a perforated Solar Array Wing. During the spacewalk, the astronaut also cut a snagged wire risking 100 V electricity. (**b**) Image of a hole by orbital debris in a panel of the Solar Max experiment. The impact craters on the aluminum exterior ISS handrails for spacewalks may have particularly sharp edges, representing a real risk of damage to the gloves of pressure suits. A new generation of composites based on bio-inspired and 2D nanomaterials will be fundamental for reducing risk of fatal hazard in long human space missions, e.g., to Mars (Images: NASA Orbital Debris Program Office)

tough backing layers absorb the residual kinetic energy by fiber/matrix failure and delamination [6–9]. Nowadays, in the era of nanomaterials we are moving towards atomistic scale two-dimensional (2D) materials, like graphene, coupling high resistance [10] and flaw tolerance at the nanoscale [11, 12], which could represent a breakthrough in protection levels [13, 14]. Complementary or alternatively, superior level of protection may be pursued through smart structural solutions to be employed even with traditional materials above mentioned, with all the advantages that this option implies in terms of consolidated manufacturing techniques and costs. Nature, having worked over the ages for optimizing defensive mechanisms against predators' attacks or impact loads, is one of the most inspiring sources in this sense [15].

Upon impact, several complex physical phenomena take place: elastic-plastic deformation and wave propagation, fracture and fragmentation, heat generation (by yielding and friction), changing of material properties due to strain-rate effects up to phase change. Their occurrence and magnitude depend on the impact velocity that may be very low or up to extreme values ($\geq$3 km/s for hypervelocity impact), with increasing challenges for armors protective capabilities as well as for their accurate modeling and design. The theoretical description of the basic aspects of impact mechanics [16–19] has reached a level of advanced maturity only singularly but when coupled, due to the severe mathematical complexity, it is in a sort of stalemate. With high speed calculators and the development of computational methods (e.g., finite element method (FEM), meshless methods), simulation [20] has become the favorite design tool, allowing optimization studies. Furthermore, technological and economic limits in large-scale production of nanomaterials and the difficulties in their manipulation or in their structural arrangement into complex bio-inspired structures require a systematic and reliable design process able to provide a tentative target optimum. The large variety of parameters to be considered in the study of toughening

mechanisms in biological materials due to their heterogeneity, the numerous levels of hierarchy, and the complexity of the constitutive laws (also strain-rate dependent) make experimental tests scarcely viable [21]. Moreover, with mere experiments is nearly impossible to investigate the whole design space. The traditional stand-alone experimental approach for armor design according to the philosophy "add material until it stops" it is not viable any more since the addition of mass can result in even suboptimal configuration [22]. In this scenario, computational models can be powerful tools for the design of new energy absorbing materials. Although important progress has been made in the past decades to simulate damage and failure processes taking place at impact, penetration, and fragmentation, much work remains to be done. The advent of nanomaterials and bio-inspiration is further questioning the capabilities of these tools and stimulates the research in this field.

In this chapter, we review computational methods for modeling the impact behavior of materials and structures under high-velocity (e.g., ballistic) impacts, severe compression and contact. In section "Biological Armors," we review some of the main studies regarding biological and bio-inspired nanoarmors highlighting common protection mechanisms in Nature. In section "Computational Methods," we put a light on the main computational methods for modeling the mechanics of biological and bio-inspired (also hierarchical) materials for impact protection, with a particular focus on the finite element method. In the end, in section "Examples of Bio-inspired Structures for Impact Protection and Energy Absorption" we present in detail a modeling example of bio-inspired ceramic-composite armor with ballistic protection capabilities, highlighting the aspect of energy absorption scalings, and an analysis on modified honeycomb structures for energy absorption under crashing, showing the key role of simulations for these studies. This review is intended to help the readers to identify starting points for research in the field of modeling, simulation, and design of bio-inspired and hierarchical energy absorbing materials and structures.

2 Biological Armors

Many current-day animals possess armor, whose scope is to provide defense from the puncturing teeth of their predators. These include mammals (e.g., armadillo and pangolin [23]), reptiles (e.g., alligators, crocodiles, and turtles [24]) and various fishes [25, 26]. Despite the wide variation in the structure and material composition, there are distinct common aspects: the armor is generally composed of discrete rigid plates connected to the body and to each other by soft collagen fibrils and muscular tissue, which serve as back substrate [15]. This solution is able to provide an effective protection together with the required flexibility [27] for locomotion.

Among these, the dermal structure of the *Arapaima gigas* fish is one of the most widely studied bioarmors in literature due to its unique characteristics [25, 26] (Fig. 2a). Its scales are composed of inner layers of mineralized collagen fibrils arranged in lamellae forming a Bouligand pattern [28] and of a highly mineralized outer layer which both dissipate energy by fracture mechanisms. There are at least three different orientations of collagen layers providing a certain grade of isotropy in

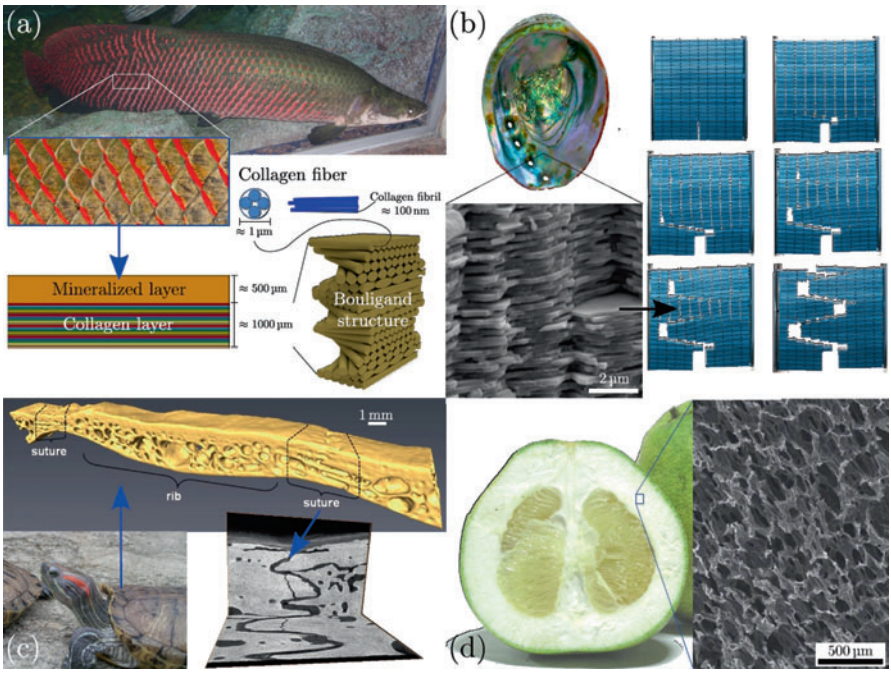

Fig. 2 Examples of natural armors and energy absorbing structures. (**a**) Multilayer and hierarchical structure of the *Arapaima gigas* scales. (**b**) Block microstructure of the nacre and example of bio-inspired composite produced via additive manufacturing showing extreme toughness a flaw-tolerance characteristics. The crack follows a long path through the specimen thus dissipating large amounts of energy (Image of 3D printed composite adapted from Ref. [42] with permission). (**c**) Red-eared slider turtle (*Trachemys Scripta Elegans*) outer shell showing zig-zag suture between adjacent non-overlapped scales (Micro-CT images adapted from Ref. [24] with permission). (**d**) Hierarchical foamy peel of the Pomelo (*Citrus Maxima*) (SEM image of the peel adapted from Ref. [85] with permission)

the tensile and bending response of the armor. Tensile tests of notched *Arapaima gigas* scales [25] have shown how the layers of collagen fibrils separate with some of them that fracture, while others remain intact. This represents an effective crack bridging, a further extrinsic toughening mechanism [29] which is widely exploited in many cross-ply fiber-reinforced polymers [30].

Other kinds of common toughening mechanism rely on the optimized hierarchical structure. For example, the mineral layer of alligator scales [31] exploits the presence of voids with optimal disposition and density that are able to deviate the crack pattern, thus increasing the toughness. Probably, the most known mechanism of this type belongs to nacre [32] (Fig. 2b). Its microstructure is mostly made of microscopic ceramic tablets densely packed and bonded together by a thin layer of biopolymer. Material properties are properly calibrated and coupled in synergy with the structural arrangement, so that the crack propagation is constricted within the

polymer phase by continuing to change the direction of propagation. When the crack has completely passed through, a further reservoir of toughness is available due to the interlocking between the lamellae. This hierarchical structure coupled with material of different characteristics (e.g., stiffness) is another common characteristic in natural structures and has been demonstrated to be the key for such extreme toughness and flaw tolerance [33]. The importance of material mixing has been demonstrated to be fundamental through numerical simulations showing that hierarchy per se is not beneficial for increasing strength and toughness, but must be necessarily coupled with material heterogeneity within the same hierarchical lever or at different scales [34]. These concepts have been widely exploited for the realization of bio-inspired composites with enhanced toughness [35].

The effective protection of these armors does not rely only on the optimized hierarchical microstructure but also the macroscopic arrangement has an important role, especially in mitigating the pain in the inner tissues of the animal. The scale-based structure has been implemented in different animals to provide the required flexibility with specific variants. In the armadillo carapace [36], the elements are hexagonal in the pectoral part and not overlapped, with collagen fibers connecting to the adjoining osteoderms. In the alligator gar and Senegal bichir, the bony scales have some overlap and the exposed (non-overlapped) regions are covered with ganoine [31]. In the red-eared slider turtle (*Trachemys Scripta Elegans*), sutures forming a zig-zag pattern ensure a minimum of non-bone area and flexibility [37] (Fig. 2c). These hierarchical sutures provide also a way of energy dissipation through local deformation and friction and could represent a further source of optimization in bio-inspired armors [38]. The analysis of scales subjected to transverse compression and the evaluation of the distribution of stresses towards the substrate have been carried out in a fundamental work by Vernerey and Barthelat [39]. They concluded that the scale mechanism provides a strain-stiffening structure, and this is a strategy to prevent structural damage and failure. Comparing different scales, ligament rigidity, and grade of overlap they demonstrated how it is possible to obtain a wide spectrum of constitutive responses, optimized for the specific load. It is interesting to mention that the scale armor concept has been used since antiquity by humans. Individual elements (in metal or leather) sewn or laced to a backing in a form of overlapping rows resembling the scales of a fish/reptile have been extensively used by Roman, Bizantine, and Japanese warriors.

Different kinds of loads correspond to different structures. While against puncturing predators' teeth and high concentrated loads, the presence of voids generally represents a weakness in the armor, a porous structure may be beneficial under distributed loads, allowing high energy dissipation through the activation of buckling deformation mechanisms in the struts of the lattice. This solution is particularly frequent in non-animal armors where the problem of flexibility and armor ergonomics (also thickness) is of second importance. A meaningful example is the hierarchical structure of the foamy peel of the Pomelo fruits (*Citrus maxima*) [40] that are able to withstand impact forces resulting from falls of over 10 m (≈100–200 J) without damage. The fruit toughness is due to the graded hierarchical fiber-reinforced composite foam (Fig. 2d). The foams struts, which are cells from the biological

point of view, consist of liquid-filled cores and shells (cell walls) with relatively high strength. Recently, an effective aluminum-based cast composite inspired by this structure has been proposed [41]. In section "Examples of Bio-inspired Structures for Impact Protection and Energy Absorption," an example of analogous honeycomb-like lattice is presented, highlighting in detail the various dissipation mechanism in this kind of structures.

When dealing with bio-inspired armors, complex architectural geometries, multiscale fracture and instabilities phenomena may arise through the different hierarchical levels. These must be properly modeled in order to achieve reliable predictions on their behavior and on their protective capability and to perform optimization analyses as well. In the next section, computational models to describe the mechanics of hierarchical material for armors and to model impact phenomena at different size scales are discussed.

3 Computational Methods

A clear understanding of the constitutive behavior of biological hierarchical material presented in the previous section and of their structural arrangement – or of their bio-inspired engineered counterpart as well – is fundamental for their implementation in an impact simulation model. Computational methods for the characterization of hierarchical materials and for the modeling of their impact mechanics need to span the various size and time scales of the problems involved. These can be divided schematically into three broad categories:

1. nanoscale methods such as density functional theory (DFT) and molecular dynamics (MD) to achieve characterization of the basic one-dimensional (1D) and two-dimensional (2D) constituents of hierarchical composites and evaluate the role of defects at this scale;
2. micro- or mesoscale fiber bundle model (FBM), lattice spring model (LSM), discrete and meshless methods to reconstruct the role of hierarchy and material mixing on the multiscale mechanical properties of composites, also including statistics;
3. meso- and macroscale finite element methods and discrete/meshless methods to model complex mechanical problems at the continuum level in solids.

Figure 3 depicts the overall scenario of computational methods in mechanics for an ideal multiscale characterization of materials for impact analysis. The methods are here briefly discussed in the following subsections.

3.1 Atomistic Simulations

The employment of nanomaterial, such as carbon nanotubes or graphene flakes, in hierarchical bio-inspired composites requires the full understanding of the mechanical behavior starting from the lowest dimensional level (Fig. 4). Molecular

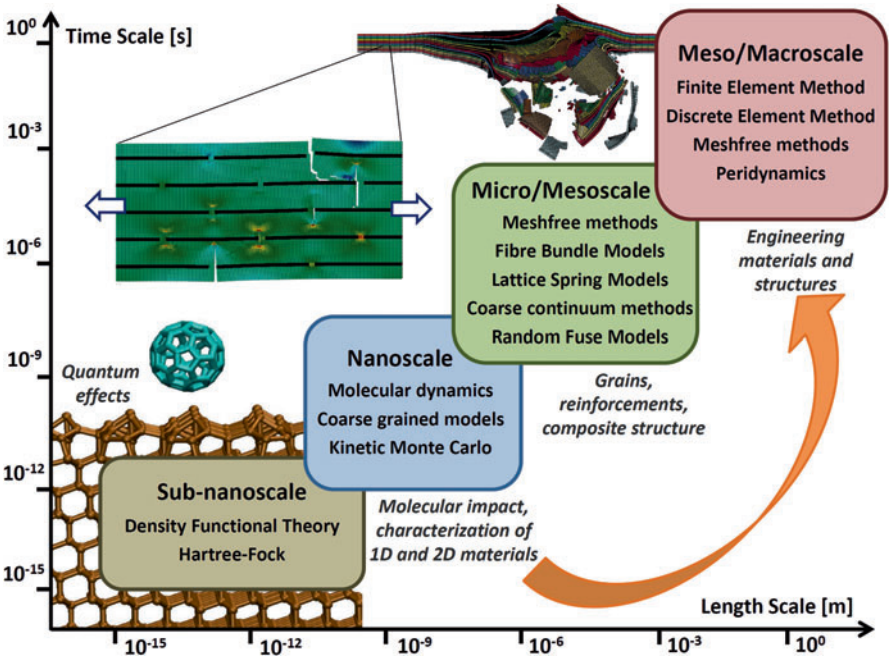

Fig. 3 Computational approaches to perform multiscale characterization of hierarchical biological and bio-inspired materials for application in armors and to model impacts at different scales. Region of applicability in spatial and timescales are indicated. Characteristic simulation are shown for the three main dimensional scales: (1) nanoscale DFT simulation of graphene production by supersonic beam epitaxy of a fullerene molecule (Image adapted under CC-BY 4.0 license from Ref. [43]); (2) mesoscale hierarchical lattice spring model (HLSM) simulation to investigate the tensile and fracture properties of a matrix embedding rigid inclusions (Image adapted under CC-BY 4.0 license from Ref. [44]), and macroscale FEM impact simulation of a steel fragment penetrating a Kevlar-based multilayer composite armor

dynamics is a simulation technique that consists of numerically solving the classical Newton's equation of motion for a set of atoms, which are characterized by their position, velocity, and acceleration. After the definition of the initial conditions of the system (temperature, number of particles, density, simulation time step, etc.), the initial equilibrium of the system is found and then the perturbation to be studied is introduced into the system. Each atom is considered as a classical particle that obeys Newton's laws of motion in relation to the interaction with other atoms which are defined by the so-called interatomic potentials (or force fields) that describe attractive and repulsive forces in between pairs and larger groups of atoms [45]. Potentials may be defined at many levels of physical accuracy; those most commonly used are based on molecular mechanics which can reproduce structural and conformational changes but usually cannot reproduce chemical reactions. When finer levels of detail are needed, potentials based on quantum mechanics (DFT) are used; some methods attempt to create hybrid classical/quantum potentials where the bulk of the system is

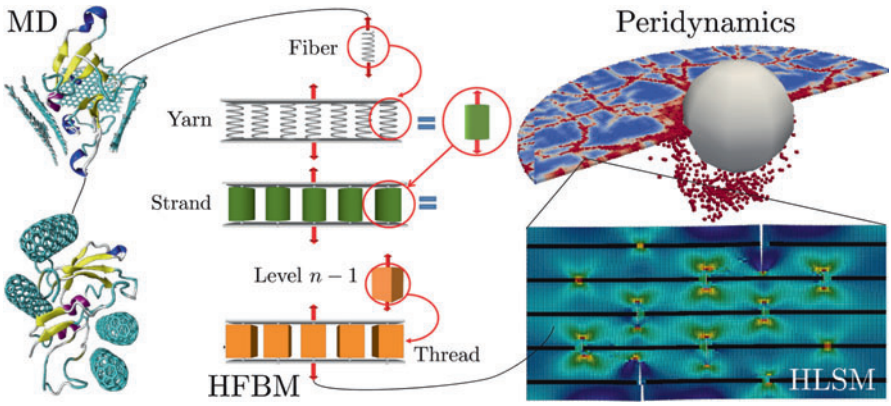

Fig. 4 Schematical representation showing the merging of different computational methods at different scale levels for the characterization of biological and bio-inspired hierarchical materials for impact simulations HLSM, HFBM and MD (HLSM image adapted from Ref. [44] under the Creative Commons BY 4.0 terms, MD image adapted from Ref. [69], with permission)

treated classically but a small region is treated as a quantum system, usually undergoing a chemical transformation.

DFT framework, based on quantum theories of electronic structure, is currently the most commonly employed quantum mechanics method, which has evolved into a powerful tool for computing electronic ground-state properties of a large number of nanomaterials. The entire field of DFT method relies on the theorem that the ground-state energy of a many-electron system is a unique and variational functional of the electron density, and this conceptual proposal is implemented in a mathematical form to solve the Kohn-Sham (KS) equations. Due to the level of complexity of this method, the related computational cost limits the analyses to systems of few hundreds of atoms. A further method to overcome system size limitation called density functional tight binding (DFTB) consists of a series of models that are derived from a Taylor series expansion of the KS-DFT total energy. The basic advantage is that the terms appearing in the total energy expression are parametrized to reproduce accurately high-level electronic structure calculations for several different bonding conditions and can be calculated in advance, saving then in computational cost. The DFTB method has been applied to study large molecules (e.g., biomolecules), clusters, nanostructures, and condensed-matter systems with a wide range of elements.

Atomistic method does not limit to the characterization of mechanical properties of 1D and 2D materials [46]. Impact-like phenomena such as the graphene synthesis via C_{60} supersonic beam epitaxy [47] (Fig. 3) or the hypervelocity impact properties of 2D materials armors against nanoscopic projectile [48] have been investigated via DFT while with MD it is possible to perform simulation of the impact of even microscale projectiles on graphene sheets [13, 49].

3.2 Models for Predicting Multiscale Properties of Hierarchical Materials

Various multiscale models have been developed to capture the mechanisms involved in the optimization of global material mechanical properties starting from nanoscale. One example is represented by the so-called fiber bundle models (FBM) [50] which are particularly appropriate for the simulation of fibrous materials, often occurring in biomaterials as seen in section "Biological Armors." With this approach the material structure at a certain size scale is modeled as an ensemble of fibers arranged in parallel (same level) and in series (different levels) subjected to uniaxial tension, with statistically Weibull-distributed yield and fracture strengths or strains. Usually, an equal-load-sharing hypothesis is adopted [51], while fibers fracture stresses are redistributed uniformly among the remaining in the bundle. Heterogeneous media are modeled by assigning different mechanical properties to the fibers of each bundle. A hierarchical extension is represented by the Hierarchical Fiber Bundle Model (HFBM) [51], whereby the input mechanical behavior of a subvolume or "fiber" at a given hierarchical level is statistically inferred from the average output deriving from reiterated simulations at the lower level, down to the lowest hierarchical level (Fig. 4). Results from this and other numerical implementations of HFBM show that specific hierarchical organizations can lead to increased damage resistance (e.g., self-similar fiber-reinforced matrix materials) or that the interaction between hierarchy and material heterogeneity is fundamental since homogeneous hierarchical bundles do not display improved properties [34]. The effect of defects at the different scale levels can also be considered.

Similar approaches, appropriate for 2D or 3D simulations, are the lattice spring models (LSM) or random fuse models [51], which provide a continuum description of the media through a network of discrete elements (springs). These have been used to simulate plasticity, damage propagation, and statistical distributions of avalanches of fracture events in heterogeneous materials [52]. The hierarchical lattice spring model (HLSM) extends the classical LSM [44] (Fig. 3). Other analytical theories such as the quantized fracture mechanics (QFM) [53] or atomistic methods such as MD can be coupled with these multiscale approaches, for instance, to determine constitutive laws at the lower scale as a function of atomic structure, defect content, or molecular organization.

Both theoretical models and the previously described numerical methods have shown that reinforcement organization in biological or bio-inspired composite materials can increase damage tolerance, avoiding direct crack path propagation and drastically improving the global response. Studies have focused on the influence of the structure, reinforcement shape, aspect ratio, dispersion, organization, and of mechanical properties of the constituents at various scale levels, iteratively deriving higher scale mechanical properties from lower ones, until a global material response is obtained [54]. The combined multiscale use of different computational techniques such as HFBM and HLSM has also proved to be successful in reproducing the macroscopic behavior of artificial nanocomposites such as gelatin-graphene oxide fibers [55]. Mesoscale models allow the design of composite materials exhibiting

tailored fracture properties, drawing inspiration from mineralized biological composites [42].

Another common property of biomaterials that can be easily studied and simulated is the self-healing and its effects on the elastic, fracture, and fatigue properties of materials. Self-healing can be incorporated in HFBM/HLSM models by replacing fractured fibers with intact ones (simulating the process of healing) with custom mechanical properties, volume fractions, replacement rates, and locations as damage evolves during simulations. The main control parameter is the *healing rate* defined as the ratio of the number of healed and fractured fibers in a given fixed time interval. Both distributed and local healing processes can be simulated, in case fractured fibers are replaced either over the whole structure or at specific locations where damage is accumulated, respectively [56].

Thus, HFBM and HLSM are useful in providing advanced constitutive response, including fracture, damage, and self-healing of biological and bio-inspired materials to be used as input in FEM or meshless simulations that can, therefore, be limited to the upper scale (Figs. 3 and 4). Thus, a series of parametric studies, each replicating thousands of experiments, can be performed efficiently.

3.3 Finite Element Method

One of the most widely used computational methods at the meso- and macroscale is the finite element method. The finite element formulation of the problem results in a system of algebraic equations, yielding approximate solutions at a finite number of points over the continuum domain. To solve the problem, it subdivides a large problem into smaller sub-domains that are called finite elements. The simple equations that model these finite elements are then assembled into a larger system of equations that models the entire problem. FEM uses variational methods from the calculus of variations to approximate a solution by minimizing an associated error function. Avoiding to describe in detail the theory behind the formulation of basic and advanced nonlinear finite element, which is beyond the scope of this chapter and that can be found in several fundamental books [57, 58], we here introduce some common issues in the modeling of high-velocity impact and large deformation problems, which are addressed later in the modeling examples. Nowadays, commercial software offers robust nonlinear FEM tools for the analysis of these types of large-scale problems at an acceptable computational cost, implementing advanced and highly optimized contact algorithms capable of simulating high-energy impact conditions [59].

To solve time-dependent ordinary and partial differential equations with finite element analysis, either an explicit or an implicit solution scheme can be used. The first usually represents an advantage in high-velocity impact simulations, and actually is the one employed, since the equation of motion is solved step by step by computing nodal accelerations rather than displacement, thus saving computational time and memory for the determination and allocation of the stiffness matrix. The advantage is more important as the number of degrees of freedom of the model

increases. Moreover, this method is much more stable under severe materials and geometrical nonlinearities (such as the ones deriving from contacts in soft media). However, this scheme has its counteracting disadvantage: the solving technique is only conditionally stable, which means that a sufficiently small time step must be guaranteed. If the solution becomes unstable, the error will rapidly increase at every time step and the solution will become invalid. An explicit method usually needs to have 100–10,000 times smaller time steps than an implicit technique, which is unconditionally stable, to avoid this kind of errors. The time step Δt for this method is limited by the time that the elastic wave, that arises from the loading, takes to transmit through the smallest element in the mesh of the model:

$$\Delta t = \frac{d_{\min}}{c} \tag{1}$$

where $d_{\min}$ is the smallest distance between any two nodes in an element and $c = \sqrt{\frac{E}{\rho(1-\nu^2)}}$ is the sound speed in a 2D material, here assumed for the sake of simplicity linear, elastic, and isotropic (thus defined by the elastic modulus E and the Poisson's ratio ν). This distance generally corresponds to the edge with minimum length in solid element and in thin-shell element, to the thickness in thick-shell element formulation, and to the length of a monodimensional beam element. Thus, finer discretization results in increased computational time both due to the higher degrees of freedom to be computed and to the higher number of iterations which are inversely proportional to the time step Δt. As a consequence, it is very difficult to couple disparate scale levels in the same simulation since the element size and the time step will be governed by the lowest dimensional scale. From Eq. 1 it emerges that $\Delta t \sim (E/\rho)^{-1/2}$, thus bulk materials coupling extreme high modulus and low density may represent an issue in terms of computational cost. On the other hand, materials with high specific modulus are the ideal candidates for impact protection since the energy dissipation capability of a material under ballistic impact can be assessed by the magnitude of the Cuniff's parameter $U^* = \frac{\sigma\varepsilon}{2\rho}\sqrt{\frac{E}{\rho}}$ [60, 61], which is the product of the material-specific dissipated energy times the elastic wave speed in the considered medium, and ε is the ultimate strain of the material. Common time steps for impact simulations on systems at the centimeter scales are of the order of 10^{-8} s which represents a limit for the characteristic time of the physical phenomenon to be modeled. However, this problem is partially mitigated due to the fact that the maximum characteristic time of a high-velocity impact event is of the order of few milliseconds, due to its intrinsic nature. When dealing with low velocity impacts, a common practice is to fictitiously increase the mass of the system (generally known as "mass scaling") in order to maximize the minimum time step required for stability. However, this practice must be properly evaluated and only exploited when the kinetic energy of the system is sufficiently low to be considered negligible in the specific problem, such as in quasi-static simulations.

Given the fine discretization that may be required in order to accurately simulate impact phenomena, usually under integrated elements are preferred over fully

integrated formulations to reduce the computational cost of the model and compensate the previous issues. For the function to be integrated to find the solution of the finite element problem, a number of points are calculated, known as Gaussian coordinates, whose position within the element is optimized for the highest grade of precision of the quadrature rule used to approximate the integrals. For each of these points, the function is multiplied by an optimized weight function. Then these are added together to calculate the integral. Reduced integration uses a lower number of Gaussian coordinates when solving the integral. Clearly, the more Gaussian coordinates for each element, the more accurate the answer will be, but this has to be weighed up against the cost of computation time. For example, the stiffness matrix has to be calculated in just one integration point of the element in case of "one-point quadrature rule" rather than the four of a 2×2 Gauss integration. The use of fewer integration points should produce a less stiff element. This sometimes is beneficial since it counteracts the overstimated stiffness of some element formulations, and in some particularly nonlinear problems such as plasticity, creep or incompressible materials the slight loss of accuracy is counteracted by the improvement in approximation to the real experimental behavior.

Sometimes the reduction of the stiffness matrix leads to its singularity generating the so-called "sporious" or "zero-energy" modes of deformation, also known as *hourglass* modes. These modes are associated to null energy and thus can easily propagate through the mesh, producing meaningless results. They typically manifest as a patchwork of zig-zag or hourglass-like element shapes (hence the name), where individual elements are severely deformed, while the overall mesh section can be nearly undeformed. It is quite common to experience severe hourglassing that may be visually apparent without magnification of the displacements. Generally, this kind of modes are mostly prone to be generated by concentrated loads or contact pressures. Hourglass can be faced in several methods: by inserting an artificial stiffness to the hourglass deformation modes (the default way utilized in static/quasi-static problems), by inserting an artificial viscosity (preferred for dynamic and high-velocity impact problems), by using fully integrated elements (but more expensive and less robust), or by refining the mesh (computationally expensive). Sometimes proper boundary conditions can avoid the formation of these modes due to enforced displacement compatibility. The basic hourglass control methodologies have been pioneered by Belytschko and coworkers [62]. The employment of the first two solutions, which have a negligible additional computational cost, requires a careful check in order to verify that the fictitious forces introduced to contain spurious mode of deformation are associated to a contained work that could drag physical energy from the system. Consequently, according to a widely acknowledged "rule of thumb," the hourglass energy must be lower than 10% (but the lower is better) of the strain energy to consider the simulation accurate. This condition must hold for the whole model and for each of its subparts, identified by different structural elements, material model or element formulation.

Some of the remaining issues of grid-based methods in modeling impact and large deformation problems are related to dealing with material separation (fragmentation) and capturing inhomogeneities in the deformation, leading to fracture

and material failure. One possible solution to treat fracture are erosion algorithms: in these approaches, the elements of the model are deleted from the simulation when the material reaches the imposed failure condition in a prescribed number of integration points. The energies (deformation, kinetic, etc.) associated to the deleted elements are properly stored and accounted in the energy balance, but these portions of material are not able to interact any more with the rest of the medium. Stress concentration arises around the created discontinuities and fractures can then nucleate and propagate as subsequence of element deletions. It is clear how the propagation pattern of fracture is highly dependent on the size and geometry of the mesh, which requires a proper convergence analysis. While this approach can be acceptable in impact simulations of ductile materials, leading to satisfying results for sufficiently fine meshes, it represents an intrinsic strong limit when dealing with brittle materials or in those models whose scope is to characterize the fracture parameters (e.g., toughness) by subjecting the specimen to tension, without imposing a priori a defect in the structure. To a certain extent, these problems are addressed by mesh-free (or meshless) methods reviewed next.

3.4 Meshless Methods and Peridynamics Implementation

Mesh-free methods are numerical techniques in which there is no fixed connectivity between the discretization nodes, and they are advantageous when simulating impact failure, penetration, and fragmentation. The level of nonlocality of interaction is defined by the "horizon" radius δ which defines the nodes within the generated spatial sphere to be assigned as neighbor of the reference node. Mesh-free methods can be developed for continuum (solids and fluids) or for particle-based (granular materials) formulations.

A new nonlocal method for modeling continuous media, the so-called *peridynamics*, has been specifically proposed [63] for modeling multiple interacting fractures in the dynamic regime. Unlike the partial differential equation of the standard theory, the integral equations of peridynamics are applicable even when cracks and other singularities appear in the deformation field. Thus, the continuous and the discontinuous media can be modeled with a single set of equations with the capability to model the spontaneous formation of cracks.

Peridynamics naturally leads to a meshless framework which is well suitable for the simulation of high-energy impacts involving penetration and fragmentation [64]. This has already been implemented in the acknowledged molecular dynamics code LAMMPS (Large Atomistic Massive Molecular Package Software) [65] enabling simulations at mesoscopic or even macroscopic length and timescales [66]. Examples of impact of a rigid sphere on a brittle solid show the formation of shear cone matching well with the experimental evidence (Fig. 4). Peridynamics especially suits for the modeling of elastic-brittle materials. However, successful simulations have already been performed on viscoelastic materials, thin membranes, and rods [67]. Since the theory is relatively recent and both the theoretical and the numerical frameworks are still limited to few works, its effective application to a

wide class of biomaterials (e.g., hyperelastic like) has yet to be performed. However, the literature in the field is in constant and high-rate update. Recently, the coupling with a finite element scheme has been succesfully applied also to impact simulations [68], showing the concrete possibility of a real multiscale approach from atomistic to continuum.

4 Examples of Bio-Inspired Structures for Impact Protection and Energy Absorption

In this section, two meaningful examples of energy absorbing structures are presented. The first is a multilayer ceramic-composite armor inspired by the structure of dermal armor scales presented in section "Biological Armors." This represents an example of structure which asbsorbs kinetic energy by material failure. The second example is a modified honeycomb concept, whose toughness relies on the combination of severe plastic deformation and buckling instability.

4.1 Ceramic-Composite Armor Under Ballistic Impact

Ceramic armors are used for the containment of blast fragments and were developed specifically for the prevention of projectile penetration, thanks to a high hardness and compressive strength with a sensible advantage of light weight ($\rho = 2500 - 3000$ kg/m^3) with respect to metallic materials. Generally, they are coupled with a backing multilayer structure of fiber/matrix composite materials with the scope of absorbing the residual kinetic energy of the generated fragments [6]. This solution is very similar to the scale structure of natural armors presented in section "Biological Armors" and represents an example of engineering bio-inspiration. One of the first questions that may arise is why the backing collagen layer of those scales is constituted by a multilayer rather than a bulk of soft materials, considering that the orientation arrangement provides overall isotropic properties. Moreover, the growth of a multilayer structure is energetically more demanding, thus not optimized from the mere biological point of view and some structural advantages should explain this particular solution.

In order to answer this concern, we can consider a multilayer medium made up of N plies of thickness t. For the sake of simplicity, we consider here a linear elastic and isotropic material. We can describe the penetration phenomenon of a mass m by means of a simple model based on conservation of momentum. Considering just one layer and a rigid projectile, the impact kinetic energy is dissipated in a volume defined by the layer thickness t and the projectile imprint radius r:

$$\frac{1}{2}m\left(v_0^2 - v_{\text{res}}^2\right) = \eta\sigma\pi r^2 t \tag{2}$$

where v_0 is the initial projectile impact velocity, v_{res} its residual value after penetration, and σ is the impact strength of the material. η is a corrective factor, here assumed equal to unity, which takes into account dissipation phenomena not considered here such as projectile damage, delamination, and damage of the target outside the projectile imprint area. Generally, material strength shows strain-rate dependency, that in the most simple way can be taken into account as a quadratic form of the impact velocity:

$$\sigma = \sigma_0 \left[a_0 + a_1 \left(\frac{v}{v^*} \right) + a_2 \left(\frac{v}{v^*} \right)^2 \right], \tag{3}$$

where $v^* = \sqrt{\sigma_0/\rho}$ [70] is the reference velocity, function of the static monoaxial compression strength of the material σ_0 and of its density ρ in the undeformed state; a_0, a_1, and a_2 are dimensionless coefficients that modify the plate strength taking into account the projectile shape effects and friction [71]. The linear term is usually neglected in accordance with experimental results [3]. Eq. 2 can be applied for a sequence of N layers, assuming as initial impact velocity on the i-th layer, the projectile residual velocity $v_{i\text{-}1}$ after the passage through the (i-1)-th layer. After some algebraic calculations, the velocity profile is given by the following relation [22]:

$$v_i = \sqrt{\frac{\left(v_i^*\right)^2}{a_{2,i}} \left\{ \exp\left[-2a_{2,i} \frac{\sigma_{0,i} \pi r^2 t_i}{m \left(v_i^*\right)^2} \right] \left[a_{0,i} + a_{2,i} \left(\frac{v_{i\text{-}1}}{v_i^*} \right)^2 \right] - a_{0,i} \right\}}, \tag{4}$$

which is valid when the expression under the square root is positive or equal to zero. If the previous condition is not satisfied, it means that the projectile has been stopped by the i-th layer and the corresponding final depth of penetration H can be calculated as follows, accordingly to Eq. 4:

$$H = \frac{m \left(v_i^*\right)^2}{2a_{2,i}\sigma_{0,i}\pi r^2} \ln\left[1 + \frac{a_{2,i}}{a_{0,i}} \left(\frac{v_{i\text{-}1}}{v_i^*} \right)^2 \right] + \sum_{n=1}^{i-1} t_n, \tag{5}$$

Consistently, the higher impactor mass m or velocity v_0 (thus higher impact kinetic energy) results in higher perforation, while higher target impact strength σ and impactor imprint radius r to lower depth of penetration. Note that with Eq. 4 it is possible to determine the velocity profile of the projectile into the target. The model is also in accordance with the predictions of the Cuniff's criterion [60] providing lower residual velocities and depth of penetration as $v^* = \sqrt{\sigma_0/\rho}$ increases.

A natural consequence of the strain-rate dependency is that the backing layers are expected to dissipate a lower amount of energy since $K_{abs} \sim \sigma \sim v^2$. Thus, it emerges from the strain-rate formulation and the multilayer impact model that the addition of material, net of other dissipation mechanisms, may be suboptimal. Considering the specific absorbed energy per layer, this concept of scaling can be analytically rationalized as follows:

$$\frac{K_{\text{abs}}}{N} = kN^{\alpha}. \tag{6}$$

A scaling exponent $\alpha > 0$ indicates a synergistic behavior in which single layers interact to mutually enhance their specific contribution. For $\alpha = 0$, the total absorbed energy is simply the sum of single-layer contributions, while for $\alpha < 0$ a suboptimal behavior is identified in which the available toughness of the materials is not fully exploited. The latter condition, although may be not intuitive, has been experimentally observed in ref. [72] -but there not interpreted- on multilayer composite targets where the sign of α appeared to be related to the adhesive properties between the layers.

In order to investigate this aspect, numerical simulation is very useful. With respect to experiments, it is possible to have precise measurement on the key variables such as the absorbed energy or the depth of penetration in the bulk, which otherwise would require sophisticated setup or time-consuming procedures. Moreover, it is possible to have full control on the interlayer adhesive properties and their variation in order to perform a precise sensitivity analysis, univocally correlating the input with the output. With simulation the amount of energy dissipated by different phenomena and different layer can be easily discriminated, giving a comprehensive understanding of the mechanics of impacts. Last but not least, it allows to simulate a sufficient high number of combinations, without time and cost demanding physical prototyping. To argue the role of interfaces, we here present a model of a typical ceramic-composite armor.

The ceramic part of the studied target is made of silicon-carbide (B_4C) modeled with the Johnson-Holmquist JH-II material model [73] implementing damage and strain-rate effects, whose parameter can be found elsewhere [74]. The model allows for progressive damage, taking into account residual material strength and compressive bulking. The thickness ratio of the two-component composite plate was set according to the results of ref. [75] where it was concluded upon experimental results that the optimum ratio in order to maximize the energy absorption, i.e., the plate ballistic limit, is given by the following relation $t_1/t_2 = 4 \cdot \rho_2/\rho_1$ where t_1 and t_2 are the ceramic and composite thicknesses, respectively, ρ_1 and ρ_2 the corresponding material densities. For the Kevlar multilayer composite backing, thick-shell elements were used (Fig. 5). This kind of elements are more suitable with respect to solids to capture the bending of thin parts with a limited number of through-thickness element and can be used in those situation where the aspect ratio of the element does not allow the use of classical thin-shell element formulations. Since in these elements the thickness is a geometrical quantity, unlike in the classical thin-shell formulations, it is possible to compute with accuracy the element deformation in the out-of-plane, dimension (thickness), making them ideal for treating the high compressive contact stresses generated by transverse impact. In the layered variant of the thick-shell formulation, it is possible to assign an arbitrary number of integration point in the element thickness and attribute to each of them a different constitutive law (woven textile or matrix) according to the volumetric fraction of the composite ply (Fig. 5). For modeling both the fiber and the matrix fractions, an orthotropic material model was used which allows to set the behavior in tension, compression, and shear along

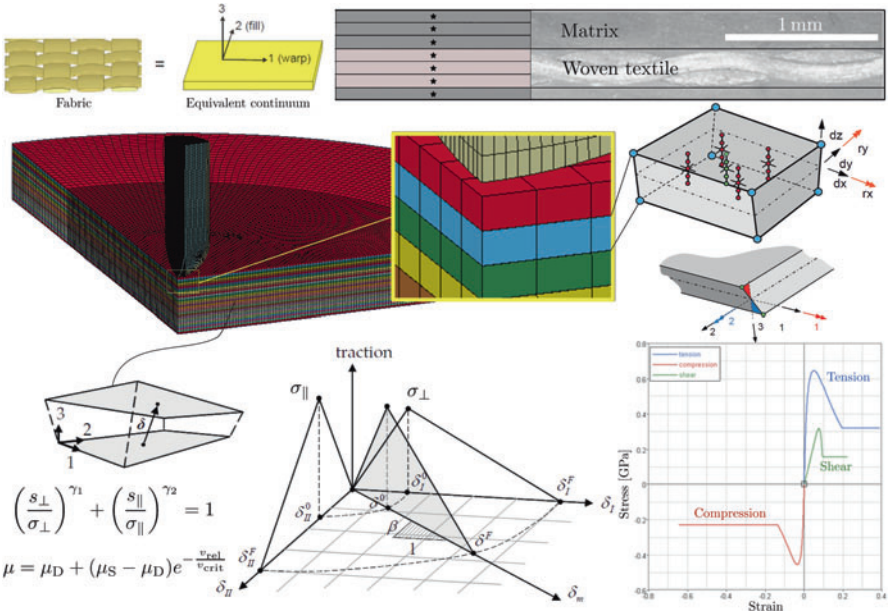

Fig. 5 Schematic representation of the modeling of the composite part of the analyzed armor. The real woven fabric immersed in the thermoset resin is modeled as a continuum equivalent medium. The two phases of the composite, fibers and matrix, are considered in the model ply introducing to each through-thickness integration different material models or properties according to the volume fraction of each phase. As a consequence of the production techniques, the ply can be seen as formed by an inner core with the properties of the woven and the outer part filled by the matix, as confirmed by the SEM photograph. Qualitative representations of the stress-separation law of the adhesive interface (bottom-left) including friction and of the constitutive behavior of the woven textile phase (bottom right) used in the simulation are also depicted

the two orthogonal in-plane directions and the out-of-plane one. The model implements a linear-elastic branch followed by a nonlinear post-peak softening behavior: the residual strength in compression, tension, and shear can be defined as a fraction of the maximum material peak stress allowing for post-peak dissipation capability. The equations which define the failure criteria used for the model are presented in detail in the paper by Matzenmiller and coworkers [76].

The adhesive contact interactions between the different plies are implemented with a so-called *tiebreak* contact. Considering a couple of adjacent nodes belonging to two subsequent layers, these are initially bonded together and the contact interface can sustain tractions. A stress-based constitutive law is implemented to define the constitutive behavior of the interface. The adhesive interface fails when the following condition is satisfied:

$$\left(\frac{s_\perp}{\sigma_\perp}\right)^2 + \left(\frac{s_\parallel}{\sigma_\parallel}\right)^2 = 1 \tag{7}$$

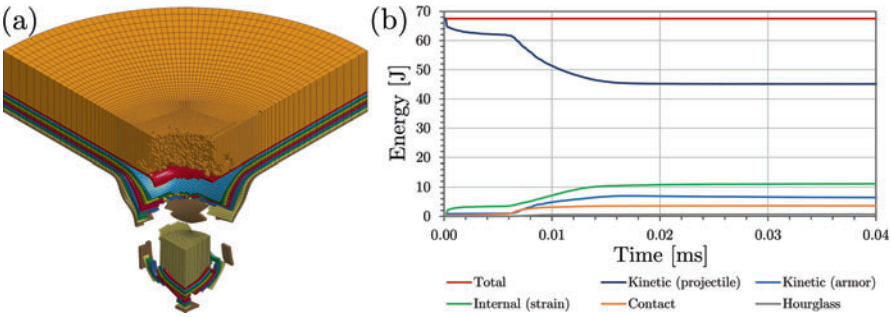

Fig. 6 Results of the FEM simulation of a steel fragment impacting a ceramic-composite armor at 350 m/s. (**a**) Picture of the armor after complete penetration (only one quarter modeled due to symmetry) showing also generation of fragments, thanks to the implementation of an erosion algorithm. Note how the mesh density is variable, having smaller element dimension under the impact region to help in containing hourglass modes and obtain a more accurate response in relation to contact stability. The radius of the analyzed plate is ≈ 6 times the projectile radius: this lower-bound is acknowledged to be sufficient to avoid edge effects in high-velocity impact phenomena (Image adapted from ref. [22] with permission). (**b**) Typical energy output from impact simulations showing how the total energy of the system is preserved. The loss of kinetic energy of the projectile (K_{abs}) goes into target deformation (internal strain energy) and contact dissipation by interface failure and friction (contact energy) and kinetic energy of the armor layers. Hourglass is within the 10% of the system internal energy thus does not affect the results significantly. Note how the ceramic absorbs a limited amount of kinetic energy (first jump in the internal and kinetic energy) with respect to the backing layers (second jump) being its primary scope to damage the projectile rather than absorb energy

where $s_\perp$ and $s_\parallel$ are the current normal and tangential stress between two welded interface nodes, while $\sigma_\perp$ and $\sigma_\parallel$ are their corresponding limit values, which may be different defining an elliptic domain. To fully define the constitutive behavior of the interface, it is also necessary to set a critical separation δ_0 for the two opening modes of the interface, after which the force can decrease until a failure nodal separation δ_f, accounting for progressive damage (Fig. 5), or suddenly drop to zero ($\delta_f = \delta_0$). Note that Eq. 7 is analogous to a cohesive zone model where stresses are placed by the current and critical fracture energies G. Here, the stress-based solution is used due to the fact that in the dynamic regime it is not straightforward to experimentally compute the critical fracture energies and thus perform a calibration of the FEM model. Once the nodes have separated, the contact locally switches to a penalty algorithm and the layers can mutually interact with friction. The law used in the contact model to compute the current kinetic friction coefficient as a function of the local static and dynamic values, μ_S and μ_D respectively, assumes the expression $\mu = \mu_S + (\mu_S - \mu_D)e^{-v_{rel}/v_{crit}}$ and is a function of the relative sliding velocity v_{rel} of the nodes-segment in contact.

Figure 6a shows a snapshot of the perforated target under the impact of a steel fragment moving at 350 m/s. A typical energy output of the simulations is depicted in Fig. 6b showing the perfect conservation of the total energy of the system, depicting the different forms of dissipations and the limitation of hourglass energy within acceptable values.

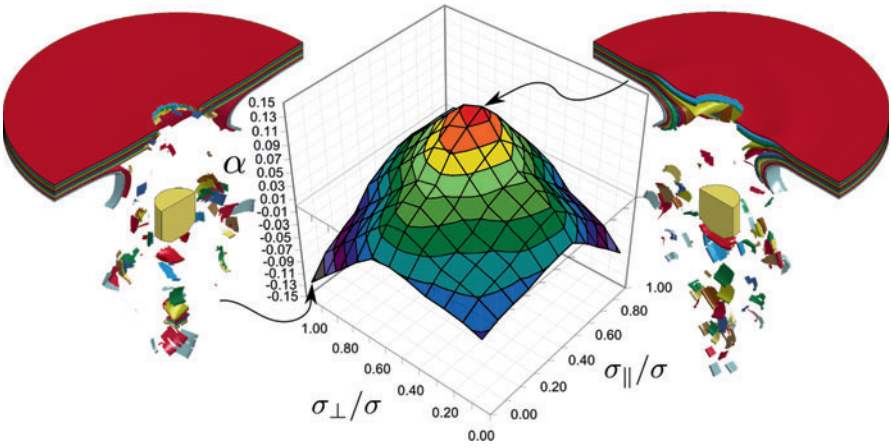

Fig. 7 Role of interface properties on the variation of the exponent α of the specific absorbed energy scaling power law (Eq. 6) in perforated multilayer composite panels. The adhesive normal and shear limit stresses, $\sigma_\perp$ and $\sigma_\parallel$ respectively, are normalized to the homogenized tensile stress of the plate. Results of impact FEM simulations show the existence of optimal interface parameters that increase and maximize the scaling of specific energy absorption (i.e., maximize α in the scaling law $\frac{K_{abs}}{N} \sim N^\alpha$), influencing the interaction of layers and their failure behavior. This explains controversial experimental observation of α for plates with different curing conditions (pressure and temperature) during the production process [72]. Each point of the graph was computed extracting the scaling exponent from sets of 6 simulations with different number of layers N resulting in overall 726 simulations. Such a number of experimental trials would be extremely difficult to perform (Image adapted from Ref. [22] with permission)

The model is exploited to perform an extensive simulation campaign to investigate the scaling in energy absorption of the composite backing multilayer. Figure 7 shows the results of the variation of the scaling exponent α (Eq. 6) as a function of the two parameters defining the adhesive properties, normalized with respect to the homogenized tensile strength of the layers σ. Each of the point in the graph is obtained by best fit of the curve $K_{abs}/N - N$ built on a basis of six simulations with $N = 2, 4, 6, 8, 10, 12$. The results clearly show how the scaling exponent can be made positive and even maximized by properly tuning the adhesive properties. A very weak interface (limit case of no adhesive interaction) may yield to $\alpha \leq 0$ in case that a synergistic coupling does not occur. Negative values are obtained also for very strong interactions $\sigma_\parallel/\sigma, \sigma_\perp/\sigma \to 1$. This can be explained with the fact that the strong interaction limits the deformation of the layers making the overall armor stiffer and with a monolithic behavior. As can be seen from Fig. 7, when the interface is very strong the bullet creates a perfect hole with amplitude nearly equal to the projectile radius while the rest of the plate is nearly undeformed, thus does not dissipate much energy. The optimal solution is obtained for intermediate situations where the tailored adhesive properties allow the layers to deform and spread damage over a wider area. From this results it is possible to understand the importance of the adhesive in governing the deformation of the target rather than dissipating energy by delamination, which is a little fraction of

the energy dissipated by permanent deformation and fracture (Fig. 6b). This result can rationalize experimental observation reported, for example, in ref. [72] where cured multilayer during the production process showed both negative and positive scaling, while non-cured plates (no adhesion between the layers) all showed suboptimal configuration for increasing areal density.

4.2 Hollow-Cylindrical-Joint Honeycombs

We here present examples of simulations of modified honeycomb structures made of a metallic alloy, subjected compressive crushing and experiencing yielding, elastic-plastic instability, and fracture. These structures could in principle be realized also with other materials (e.g., traditional composite materials, graphene-based composite, silk-like artificial materials). However, the main aim of this part, rather than simulating the behavior of a specific material, is to show the importance of simulation in integrating – and also partially substituting – experimental analyses and prototyping.

Hollow-cylindrical-joint honeycombs represent a modification of traditional honeycombs where the joints formed by the intersection of converging walls are placed by hollow cylinders (Fig. 8c). These kind of structures belong to the family of center-symmetrical hexagonal honeycombs [77] and have been recently proposed [78, 79] as possible and effective modification of conventional honeycomb structures (Fig. 8a, b) to further increase their specific mechanical properties, i.e., the yield strength (σ/ρ), stiffness (E/ρ), and toughness. It has analytically been proved that these characteristic quantities can be maximized, on an equal mass basis, in relation to specific geometric sizing of the radius r of the cylinders and of the length l of the walls (Fig. 8). In particular, an optimal (maximum) value of the mechanical properties was analytically predicted for aspect ratios $r/l \approx 0.3$ [78] (Fig. 8c).

The analytical models [78, 79] which describe the mechanics of these modified honeycombs are based on geometrical considerations and on the elastic theory of plates and shells and, thus, are limited to the description of the elastic regime. The high complexity of phenomena within the material, which experiences yielding,

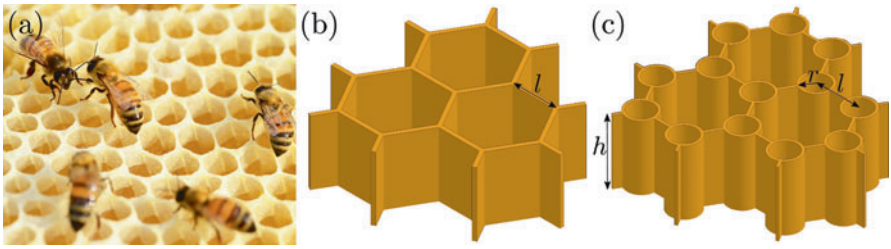

Fig. 8 From traditional to modified honeycombs. (**a**) Natural honeycomb structure of a beehive. (**b**) Reference model of a conventional regular hexagonal honeycomb structure. (**c**) Model of a hollow-cylindrical-joint honeycomb structure. Geometrical characteristics of the honeycombs are identified in the figure

elastic-plastic instabilities, and fracture under large strain and strain-rate, in addition to the geometrical nonlinearity introduced by the complex 3D geometry, requires the use of advanced simulation, in order to thoroughly describe the mechanical behavior of such honeycombs up to crushing. Further advantages are associated with the virtual modeling: the closed cell structure of the honeycombs does not allow to directly visualize the formation and the evolution of plastic folds and fractures during the experiments. Moreover, simulations can go beyond the mere measurement of the force displacement curves being able to measure other important quantities such as local stresses and strain (and thus underline with precision yielded and damaged regions), to visualize the formation of shear bands, and to precisely control and evaluate the role of different frictional properties (static and dynamic coefficient of friction) at the contact interfaces on the overall behavior.

A series of five specimen with different r/l from 0 to 0.5 and same mass was experimentally tested. Defining ρ_h/ρ_{bulk} as the ratio between the honeycomb density and the density of the constituent bulk material, the thickness of each samples to keep their mass constant can be calculated as a function of r/l according to the relation $\rho/\rho_{bulk} = -1.155(t/l)^2 + [2.528(r/l) + 1.155](t/l)$ [78]. The samples utilized for this study [79] were made using 6061-T4 aluminum alloy for the bulk constituent material ($\rho_{bulk} = 2700$ kg/m^3) being the relative apparent density of the honeycomb $\rho_h/\rho_{bulk} = 0.1$ for all the tested samples. We here report the results of monoaxial compression experiments made with a 1000HDX Instron Universal Testing Machine (ITW, USA) with loading capacity of 1000 kN. The loading rates before and after the initial yield of the samples are of 1 mm/min. Conventional quantities are defined for describing the constitutive response of the honeycomb. The compressive stress is $\sigma_h = F/A$, where F is the force recorded in the load cell of the testing machine, and A is the projected convex hull area of the honeycomb samples on the plane perpendicular to the loading direction; the corresponding compressive strain is $\varepsilon_h = \Delta h/h$, where Δh is the variation of height of the specimen.

The constitutive relationship of the aluminum alloy used in the experiment was characterized by tensioning a round dog-bone specimen with circular cross-section of diameter $d = 10$ mm up to failure. The determined mechanical properties extracted from the stress–strain curve were: the Young's modulus $E = 68$ GPa, the yield strength $\sigma_u = 287$ MPa, the ultimate stress $\sigma_u = 318$ MPa, and the failure strain $\varepsilon_f = 0.121$. Although the curve can be approximated with a bilinear elastic-plastic relationship, the experimentally derived curve was directly employed. Prior to yielding, the material is assumed linear elastic with $\varepsilon_y = \sigma_y/E$. It must be mentioned that due to the size-scale effect, in the FEM model the plastic strain in the input curve $\varepsilon_{pl} = \varepsilon - \frac{\sigma_y}{E}$ was scaled from the nominal one measured from the dog-bone test by $\frac{\varepsilon_{pl,\,FEM}}{\varepsilon_{pl}} = \frac{d}{t}$ since $t \ll d$. Thus, also the ultimate strain $\varepsilon_{f,\ FEM}$ is scaled accordingly. This operation is necessary, at least for metallic alloys such as the one considered here, otherwise one would obtain unnatural brittle behavior in the simulations very far from the experiments if size-scale effects are not considered.

Regarding the choice of elements for this kind of problems, hexahedron 1-point integration solid element (constant stress) represents an effective solution. This

solution is efficient and accurate and works very well for severe deformations. For plasticity problem, at least 3 integration points should be present through the minimum dimension of the structure, thus 3 elements of this type should be used through the thickness t. Besides the saving in computational time with respect to the 8-point fully integrated element, this choice may avoid element locking. Hourglass must also be monitored with attention and mitigated, if necessary, for this elements. The use of more element through the thickness may help in this sense. The von Mises criterion was employed for yielding. Material fracture is treated via an erosion algorithm with the elements that are deleted from simulation when either one between the principal and deviatoric strain reaches the limit $\varepsilon_{f,FEM}$. Contact interactions were implemented between the steel plates and the honeycomb. Self-contact within the honeycomb parts must also be introduced in order to properly account for material densification during the crushing process. Static and dynamic coefficients of friction were, respectively, set to be $0.61-0.47$ for the honeycomb-rigid steel plate contact and $1.35-1.05$ for the self-contact, which are common values for aluminum–steel and aluminum–aluminum surfaces.

Figure 9 reports the results in terms of stress–strain curve (quantities computed as in experiments). Since it is a displacement control simulation, the load F to compute the stress σ_h is here computed from the normal component of the contact force at the

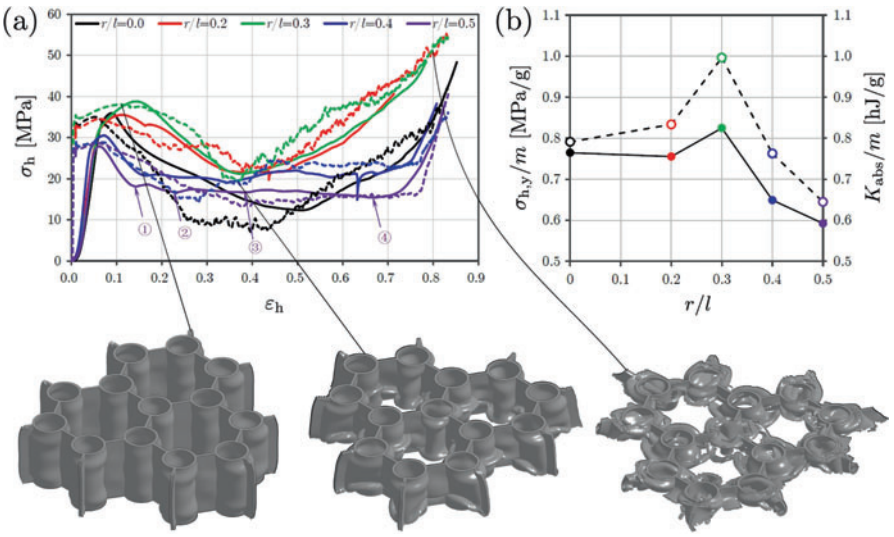

Fig. 9 (**a**) Stress–strain curves of the five simulated samples with different r/l ratios (dashed lines) and comparison with experimental results (solid lines). For $r/l = 0.5$, four states are highlighted corresponding to the images of Fig. 11b. Three simulation states for the optimal honeycomb $r/l = 0.3$ are depicted corresponding to yielding, minimum of bearing capacity, and complete fracture. (**b**) Specific yield strength (filled dots) and absorbed energy (empty dots) as a function of r/l computed from FEM simulations. Results show how the lattice is optimized for $r/l \approx 0.3$ providing the higher yield strength and energy absorption (Image adapted from Ref. [79] with permission)

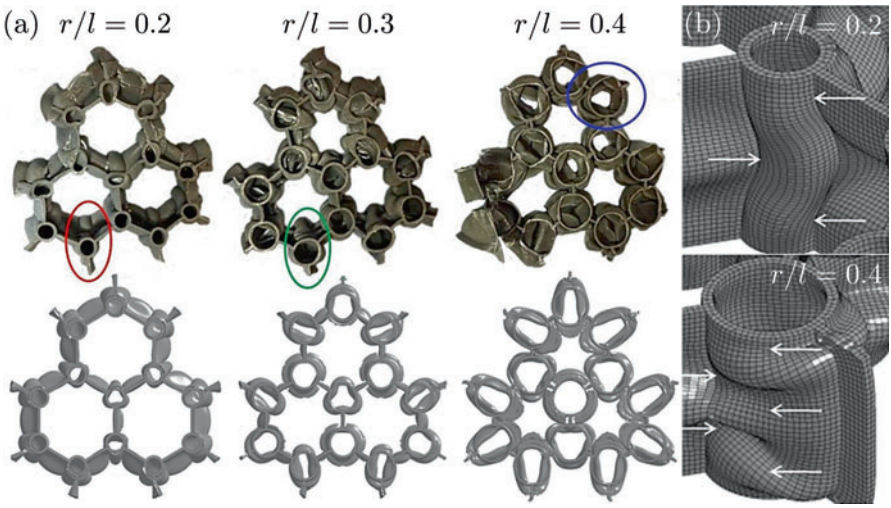

Fig. 10 (**a**) Experimental and simulated collapse modes of the out-of-plane loaded honeycombs with $r/l = 0.2$ - 0.3 - 0.4. (**b**) Snapshots of FEM simulations (at $\varepsilon_h = 20\%$) show the collapse mechanisms of the cylindrical shell-plate joint with detail of variable number of foldings for different r/l due to the mutual level of restrain between cylinders and plates and the different thickness of the honeycombs to provide the same mass (Image adapted from Ref. [79] with permission)

contact surface between the honeycomb and the steel plate, which by equilibrium is equal to the external applied load. The lattices Young's modulus, computed as $\sigma_{h,y}/\varepsilon_{h,y}$ is nearly constant, in accordance with the fact that the ratio E_h/ρ_h is a material constant [80].

The failure mechanisms obtained for the shell-plate assembled honeycombs (Fig. 10) represent a transition between the two limit behaviors of sample 1 ($r/l = 0$, classical hexagonal honeycomb) and sample 5 ($r/l = 0.5$, degenerated plates) shown in Fig. 11. The classical honeycomb, after the elastic-plastic instability of the plates, which can be approximated with the simple case of the Euler's column with both clamped edges, reaches the failure due to the formation of a sub-horizontal fracture approximately at $h/2$. For sample 5, the collapse of the structure is caused by the multiple folding of cylindrical shell and does not experience fracture. For single cylindrical tube, several works explain its collapse mechanisms, according to thickness, diameter, and length [81]. From Fig. 11a it can be seen how simulations are capable of capturing the transition between the two limit structures, with increasing number of folds and decreasing fold wavelength as r/l increases. This behavior can be imputed to the fact that for maintaining the same mass along all specimens the wall thickness t decreases with increasing r/l, yielding towards a more ductile behavior. Figure 11b gives a measure of the capability of simulation to catch large displacement deformation with the simulation deformed shape that can be nearly perfectly superposed to experimental pictures, and being able to predict the number

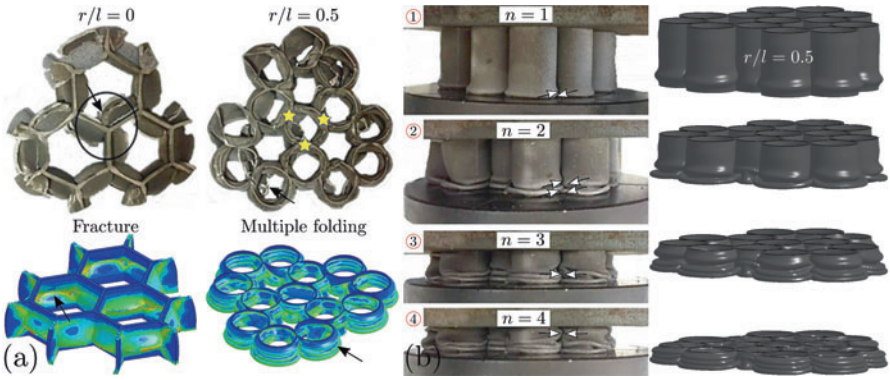

Fig. 11 (**a**) Collapse modes transition from sample 1 ($r/l = 0$, unmodified honeycomb) to sample 5 ($r/l = 0.5$, full cylindrical joint honeycomb, restrain point between the cylinders highlighted). Contour plot of plastic strain is superposed to simulated honeycomb images. (**b**) Visual comparison between crushing experiment (left) and simulation (right) on sample 5 at four deformation levels (see graph of Fig. 9a) showing very good agreement in the formation of folds (highlighted by the arrows) due to elastic-plastic instabilities. For each state, the number of folds n is indicated (Image adapted from Ref. [79] with permission)

of folds. The behavior under compression in the orthogonal (in-plane) direction was also studied in an analogous way and can be found in the related work [79].

The results indicate that the combination of hollow cylindrical shells and plates forms a new periodic assembly with better mechanical property and energy absorption capability with respect to conventional honeycombs. As shown, the developed numerical model was able to well describe the experiments, both in predicting the constitutive curves of the honeycomb behavior under compression and of the energy absorbing capabilities. Thus, the models could be used in predicting the performance of honeycombs of different geometries, further optimizing natural solutions. This concept is not limited to the here presented material but may be used to generate new crashworthy lattices at different scales, ranging from macroscopic composite sandwich panels to material structuring at the nanoscale [82, 83].

5 Conclusion

Herein, we have discussed the importance of bio-inspired structures and nanomaterials to achieve a further breakthrough for a new generation of tougher armors. Some examples of energy absorbing multilayer and lattice structures were shown, discussing the importance of simulation in solving specific problems, in understanding natural solutions and their further optimization according to engineering needs. Although numerical codes become more and more sophisticated, many problems related to the accurate prediction of real material behavior upon impact and penetration remain to be solved. The introduction of these new materials design and concepts arises further concerns regarding the ability of current computational

methods to effectively model and predict at a reasonable computational cost the impact mechanics of such protective structures, in order to compensate the limits of physical prototyping and related experimental testing. Future modeling and simulation tools will have to be able to treat concurrently and in a unified manner the many failure mechanisms present at impact and penetration, such as dynamic fracture and fragmentation, generation of dislocations, and shear bands. Some of them, such as the peridynamics, are promising in this direction. Anyhow, it must be mentioned that another crucial limit in the capability of computational analysis for the class of problems discussed here –but also for many others (e.g., fluid dynamics, astrophysics)– is the state-of-the-art in the current hardware computational architectures. Indeed, a really significant advance in the capabilities of computational analysis, in terms of model degrees of freedom and time scale, will necessarily require a breakthrough in the hardware conception [84]. Anyway, we have shown in this chapter how with the current resources it is possible to obtain significant results when different methods and theories are coupled in a synergistic way, overcoming the current limits in performing truly single-framework multiscale simulations.

Acknowledgments NMP is supported by the European Commission H2020 under the Graphene Flagship (WP14 "Polymer Composites," no. 696656) and the FET Proactive ("Neurofibers" no. 732344).

References

1. NASA. International space station risk of impact from orbital debris; 2015. http://www.nasa.gov/externalflash/iss_impact_risk/
2. Hoog PJ. Composites in armour. Science. 2006;314(5802):1100–1.
3. Abrate S. Ballistic impact on composites. In: Proceedings of the 16th International Conference on Composite Materials; Kyoto, Japan; 2007.
4. Kumar BG, Singh RP, Nakamura T. Degradation of carbon fiber-reinforced epoxy composites by ultraviolet radiation and condensation. J Compos Mater. 2002;36(24):2713–33.
5. Springer GS. Environmental effects on composite materials, vol. 3. Lancaster: Technomic Publishing; 1988.
6. Abrate S. Impact on composite structures. Cambridge/New York: Cambridge University Press; 2005.
7. Hazell PJ. Armour: materials, theory and design. Boca Raton: CRC Press; 2015.
8. LaSalvia JC, Gyekenyesi A, Halbig M. (Eds.). Advances in Ceramic Armors X. Vol. 35 of Ceramic Engineering and Science Proceedings. Wiley; 2014. ISBN: 978-1-119-04060-6.
9. Liu W, Chen Z, Chen Z, Cheng X, Wang Y, Chen X, et al. Influence of different back laminate layers on ballistic performance of ceramic composite armor. Mater Des. 2015;87:31–27.
10. Lee C, Wei X, Kysar JW, Hone J. Measurement of the elastic properties and intrinsic strength of monolayer graphene. Science. 2008;321(5887):385–8.
11. Zhang T, Li X, Kadkhodaei S, Gao H. Flaw insensitive fracture in nanocrystalline graphene. Nano Lett. 2012;12(9):4605–10.
12. Cranford SW. When is 6 less than 5? Penta- to hexa-graphene transition. Carbon. 2016;96:421–8.
13. Lee JH, Loya PE, Loeu J, Thomas EL. Dynamic mechanical behavior of multilayer graphene via supersonic projectile penetration. Science. 2014;346:1092–6.

14. Lee JH, Veysse D, Singer JP, Retsch M, Saini G, Pezeril T, et al. High strain rate deformation of layered nanocomposites. Nat Commun. 2012;3(1164):1–7.
15. Yang W, Chen IH, Gludovatz B, Zimmermann EA, Ritchie RO, Meyers MA. Natural flexible dermal armour. Adv Mater. 2013;25(1):31–48.
16. Goldsmith WJ. IMPACT – the theory and physics of colliding solids. 2nd ed. New York: Dover Publications; 2001.
17. Recht RF, Ipson TW. Ballistic perforation dynamics. J Appl Mech. 1963;30(3):384–90.
18. Goldsmith W. Non-ideal projectile impact on targets. Int J Impact Eng. 1999;22(2–3):95–395.
19. Porwal PK, Phoenix SL. Modeling system effects in ballistic impact into multi-layered fibrous materials for soft body armor. Int J Fract. 2005;135(1-4):217249.
20. Lim CT, Shim VPW, Ng YH. Finite-element modeling of the ballistic impact of fabric armor. Int J Impact Eng. 2003;28(1):13–31.
21. Signetti S, Bosia F, Pugno NM. Computational modelling of the mechanics of hierarchical materials. MRS Bull. 2016;41(9):694–9.
22. Signetti S, Pugno NM. Evidence of optimal interfaces in bio-inspired ceramic-composite panels for superior ballistic protection. J Eur Ceram Soc. 2014;34(11):2823–31.
23. Wang B, Yang W, Vincent R, Sherman R, Meyers MA. Pangolin armor: overlapping, structure, and mechanical properties of the keratinous scales. Acta Biomater. 2016;41:60–74.
24. Achrai B, Bar-On B, Wagner HD. Bending mechanics of the red-eared slider turtle carapace. J Mech Behav Biomed Mater. 2014;30:223–33.
25. Bruet BJF, Song J, Boyce MC, Ortiz C. Materials design principles of ancient fish armour. Nat Mater. 2008;7(9):748–56.
26. Yang W, Sherman VR, Gludovatz B, Mackey M, Zimmermann EA, Chang EH, et al. Protective role of Arapaima gigas fish scales: structure and mechanical behavior. Acta Biomater. 2014;5 (8):3599–614.
27. Rudykh S, Ortiz C, Boyce MC. Flexibility and protection by design: imbricated hybrid microstructures of bio-inspired armor. Soft Matter. 2015;11:2547–54.
28. Zimmermann EA, Gludovatz B, Schaible E, Dave NKN, Yang W, Meyers MA, et al. Mechanical adaptability of the Bouligand-type structure in natural dermal armour. Nat Commun. 2013;4:2634.
29. Li L, Ortiz C. A natural 3D interconnected laminated composite with enhanced damage resistance. Adv Funct Mater. 2015;25(23):3463–71.
30. Garrett KW, E J B. Multiple transverse fracture in 90° cross-ply laminates of a glass fibre-reinforced polyester. J Mater Sci. 1977;12(1):157–68.
31. Currey JD. Mechanical properties and adaptations of some less familiar bony tissues. J Mech Behav Biomed Mater. 2010;3(5):357–72.
32. Barthelat F, Tang H, Zavattieri PD, Li CM, Espinosa HD. On the mechanics of mother-of-pearl: a key feature in the material hierarchical structure. J Mech Phys Solids. 2007;55(2):306–37.
33. Sen D, Buehler MJ. Structural hierarchies define toughness and defect-tolerance despite simple and mechanically inferior brittle building blocks. Sci Rep. 2011;1(35):1–9.
34. Bosia F, Abdalrahman T, Pugno NM. Investigating the role of hierarchy on the strength of composite materials: evidence of a crucial synergy between hierarchy and material mixing. Nanoscale. 2012;4:1200–7.
35. Dimas LS, Buehler MJ. Modeling and additive manufacturing of bio-inspired composites with tunable fracture mechanical properties. Soft Matter. 2014;10:4436–42.
36. Vickaryous MK, Hall BK. Osteoderm morphology and development in the nine-banded armadillo, Dasypus novemcinctus (Mammalia, Xenarthra, Cingulata). J Morphol. 2006;267 (11):1273–83.
37. Rhee H, Horstemeyer MF, Hwang Y, Lim H, Kadiri HE, Trim W. A study on the structure and mechanical behavior of the Terrapene carolina carapace: a pathway to design bio-inspired synthetic composites. Mater Sci Eng C. 2009;29(8):2333–9.

38. Lin E, Li Y, Weaver JC, Ortiz C, Boyce MC. Tunability and enhancement of mechanical behavior with additively manufactured bio-inspired hierarchical suture interfaces. J Mater Res. 2014;29(17):1867–75.
39. Vernerey FJ, Barthelat F. On the mechanics of fishscale structures. Int J Solids Struct. 2010;47 (17):2268–75.
40. Thielen M, Schmitt CNZ, Eckert S, Speck T, Seidel R. Structure-function relationship of the foam-like pomelo peel (Citrus maxima) an inspiration for the development of biomimetic damping materials with high energy dissipation. Bioinspir Biomim. 2013;8(2):025001.
41. Fischer SF, Thielen M, Weiß P, Seidel R, Speck T, Bührig-Polaczek A, Bünck M. Production and properties of a precision-cast bio-inspired composite. J Mater Sci. 2014;49(1):43–51.
42. Dimas LS, H G B, Eylon I, Buehler MJ. Tough composites inspired by mineralized natural materials: computation, 3D printing, and testing. Adv Funct Mater. 2013;23(36):4629–38.
43. Aversa L, Taioli S, Nardo MV, Tatti T, Verrucchi R, Iannotta S. The interaction of C60 on Si (111) 7×7 studied by supersonic molecular beams: interplay between precursor kinetic energy and substrate temperature in surface activated processes. Front Mater. 2015;2(46):12–20.
44. Brély L, Bosia F, Pugno NM. A hierarchical lattice spring model to simulate the mechanics of 2-D materials-based composites. Fron Mater. 2015;2(51):64–73.
45. Frenkel D, Smit B. Understanding molecular simulation – from algorithms to applications. 2nd ed. San Diego: Academic; 2002.
46. Xu M, Paci JT, Oswald J, Belytschko T. A constitutive equation for graphene based on density functional theory. Int J Solids Struct. 2012;49(18):2582–9.
47. Tatti R, Aversa L, Verrucchi R, Cavaliere E, Garberoglio G, Pugno NM, et al. Synthesis of single layer graphene on Cu(111) by C60 supersonic molecular beam epitaxy. RSC Adv. 2016;6 (44):37982–93.
48. Signetti S, Taioli S, Pugno NM. 2D materials armors showing superior impact strength of few layers. ACS Appl Mater Inter. 2017;9(46):40820–30.
49. Yoon K, Ostadhossein A, van Duin ADT. Atomistic-scale simulations of the chemomechanical behavior of graphene under nanoprojectile impact. Carbon. 2016;99:58–64.
50. Pradhan S, Hansen A, Chakrabarti BK. Failure processes in elastic fiber bundles. Rev Mod Phys. 2010;82(1):499–555.
51. Pugno NM, Bosia F, Abdalrahman T. Hierarchical fiber bundle model to investigate the complex architectures of biological materials. Phys Rev E. 2012;85:011903.
52. Zapperi S, Vespignani A, Eugene Stanley H. Plasticity and avalanche behaviour in micro-fracturing phenomena. Nature. 1997;388(6643):658–60.
53. Pugno NM, Ruoff RS. Quantized fracture mechanics. Philos Mag. 2004;84(27):2829–45.
54. Zhang Z, Zhang YW, Gao H. On optimal hierarchy of load-bearing biological materials. Proc R Soc B. 2011;278(1705):519–25.
55. Panzavolta S, Bracci B, Gualandi C, Focarete ML, Treossi E, Kouroupis-Agalou K, et al. Structural reinforcement and failure analysis in composite nanofibers of graphene oxide and gelatin. Carbon. 2014;78:566–77.
56. Bosia F, Abdalrahman T, Pugno NM. Self-healing of hierarchical materials. Langmuir. 2014;30 (4):1123–33.
57. Belytschko T, Liu WK, Moran B, Elkhodary K. Nonlinear finite elements for continua and structures. 2nd ed. Hoboken: Wiley; 2013.
58. Wriggers P. Computational contact mechanics. 2nd ed. Berlin/Heidelberg: Springer-Verlag; 2006.
59. Hallquist JO, Goudreau GL, Benson DJ. Sliding interfaces with contact-impact in large-scale Lagrangian computations. Comput Methods Appl Mech Eng. 1985;51(1):107–37.
60. Cuniff PM. Dimensionless parameters for optimization of textile-based body armor systems. In: Proceedings of the 18th International Symposium of Ballistics. San Antonio; 1999. p. 1303–10.
61. Cuniff PM. Analysis of the system effects in woven fabrics under ballistic impact. Text Res J. 1992;62(9):495–509.

62. Belytschko T, Ong JSJ, Liu WK, Kennedy JM. Hourglass control in linear and nonlinear problems. Comput Methods Appl Mech Eng. 1984;43(3):251–76.
63. Silling SA. Reformulation of elasticity theory for discontinuities and long-range forces. J Mech Phys Solids. 2000;48(1):175–209.
64. Silling SA, Askari E. A meshfree method based on the peridynamic model of solid mechanics. Comput Struct. 2005;83(17–18):1526–35.
65. Laboratories SN. LAMMPS molecular dynamics simulator; 2015. http://lammps.sandia.gov/
66. Parks ML, Lehoucq RB, Plimpton SJ, Silling SA. Implementing peridynamics within a molecular dynamics code. Comput Phys Commun. 2008;179(11):777–83.
67. Silling SA, Bobaru F. Peridynamic modeling of membranes and fibers. Int J Non-Linear Mech. 2005;40(2–3):395–409.
68. Lee J, Liu W, Hong JW. Impact fracture analysis enhanced by contact of peridynamic and finite element formulations. Int J Impact Eng. 2016;87:108–19.
69. Lepore E, Bonaccorso F, Bruna M, Bosia F, Taioli S, Garberoglio G, et al. Silk reinforced with graphene or carbon nanotubes spun by spiders. arXiv. 2016. (arXiv:1504.06751 [cond-mat.mtrl-sci]) 2D Mater. 2017; 4(3):031013.
70. Forrestal MJ, Tzou DY. A spherical cavity-expansion penetration model for concrete targets. Int J Solids Struct. 1997;34(31–32):4127–46.
71. Ben-Dor G, Dubinsky A, Elperin T. High-speed penetration modeling and shape optimization of the projectile penetrating into concrete shields. Mech Based Des Struct Mach. 2009;37(4):538–49.
72. Jacobs MJN, Dingenen JLJV. Ballistic protection mechanisms in personal armour. J Mater Sci. 2001;36(13):3137–42.
73. Johnson GR, Holmquist TJ. An improved computational constitutive model for brittle materials. AIP Conf Proc. 1994;309(1):981–4.
74. Cronin DS, Bui K, Kauffmann C, McIntosh G, Berstad T. Implementation and validation of the Johnson-Holmquist ceramic material model in Ls-Dyna. In: 4th European LS-DYNA Users Conferences; Ulm, Germany; 2011. p. 47–60.
75. Hetherington JG. The optimization of two component composite armours. Int J Impact Eng. 1992;12(3):409–14.
76. Matzenmiller A, Lubliner J, Taylor RL. A constitutive model for anisotropic damage in fiber-composites. Mech Mater. 1995;20(2):125–52.
77. Miller W, Smith CW, Scarpa F, Evans KE. Flatwise buckling optimization of hexachiral and tetrachiral honeycombs. Compos Sci Technol. 2010;70(7):1049–56.
78. Chen Q, Pugno NM, Zhao K, Li Z. Mechanical properties of a hollow-cylindrical-joint honeycomb. Compos Struct. 2014;109:68–74.
79. Chen Q, Shi Q, Signetti S, Sun F, Li Z, Zhu F, et al. Plastic collapse of cylindrical shellplate periodic honeycombs under uniaxial compression: experimental and numerical analyses. Int J Mech Sci. 2016;111–112:125–33.
80. Gibson LJ, Ashby MF. Cellular solids – structure and properties. 2nd ed. Cambridge/New York: Cambridge University Press; 1999.
81. Andrews KRF, England GL, Ghani E. Classification of the axial collapse of cylindrical tubes under quasi-static loading. Int J Mech Sci. 1983;25:687–96.
82. Nedjari S, Schlatter G, Hébraud A. Thick electrospun honeycomb scaffolds with controlled pore size. Mater Lett. 2015;142:180–3.
83. Applegate MB, Coburn J, Partlow BP, Moreau JE, Mondia JP, Marelli B, et al. Laser-based three-dimensional multiscale micropatterning of biocompatible hydrogels for customized tissue engineering scaffolds. Proc Natl Acad Sci. 2015;112(39):12052–7.
84. de Touzalin A, Marcus C, Heijman F, Cirac I, Murray R, Calarco T. QUANTUM MANIFESTO – a new era of technology; 2016. http://qurope.eu/manifesto
85. Chen S., Liu Q, He G., et al. Reticulated Carbon Foam Derived From a Sponge-Like Natural Product as a High Performance Anode in Microbial Fuel Cells. J. Mat. Chem. 2012;22:18609–18613